Extensions and Applications of Image Metamorphosis

Sebastian Neumayer

TU Kaiserslautern

neumayer@mathematik.uni-kl.de

joint work with

A. Effland (Graz), L. Lang (Cambridge), O. Öktem (Stockholm),
J. Persch (Kaiserslautern), M. Rumpf (Bonn), C. Schönlieb (Cambridge)
and G. Steidl (Kaiserslautern)

April 3, 2019

Overview

Contents

Introduction to Morphing

Image morphing = smooth image transition

$\Longrightarrow$

How do we obtain such a smooth transition?

Linear Interpolation

Morphing models

Several possible methods:

- feature based morphing: mapping of special features; calculation of whole deformation by interpolation
  (Smythe 1990 in movie ,,Willow'', Wolberg 1998)
- flow of diffeomorphisms, large deformation diffeomorphic metric mapping (LDDMM): each image pixel is transported along a trajectory determined by a diffeomorphism path
  (Dupuis, Grenander & Miller 1998, Trouvé 1995, 1998)
- **metamorphosis**: allows variation of image intensities along pixel trajectories
  (Miller, Trouvé, Younes 2001, 2005)

Comparison of linear interpolation and metamorphosis

Comparison of linear interpolation and metamorphosis

Contents

How is a metamorphosis image path defined?

The image path is given as the minimizer of an energy functional.

Notations

- $\Omega \subset \mathbb{R}^2$: Image domain (open, bounded, Lipschitz boundary)
- $T \in L^2(\Omega)$: Template image
- $R \in L^2(\Omega)$: Target image
- $v \in \mathcal{V} := L^2((0,1), V)$: Velocity field with a reflexive Banach space $V \hookrightarrow C_0^1(\Omega)$ describing the space regularity of v, e.g. $V = H_0^3(\Omega)$
- $z \in \mathcal{Z} := L^2((0,1), L^2(\Omega))$: Source term, modeling intensity change

Metamorphosis from optimal control perspective

Metamorphosis functional

Let $\lambda_1, \lambda_2 > 0$ and $\mathcal{E}_1 \colon L^2(\Omega) \to \mathbb{R}$, $\mathcal{E}_2 \colon V \to \mathbb{R}$ be regularizers. The optimal control formulation of metamorphosis reads

$$\min_{(v,z) \in \mathcal{V} \times \mathcal{Z}} \int_0^1 \lambda_1 \mathcal{E}_1(z(t,\cdot)) + \lambda_2 \mathcal{E}_2(v(t,\cdot)) \,\mathrm{d}t + \|S(v,z) - R\|^2_{L^2(\Omega)}. \tag{1}$$

The control-to-state operator $S \colon \mathcal{V} \times \mathcal{Z} \to L^2(\Omega)$ is the solution of

$$\begin{aligned} \frac{\partial f}{\partial t} + v \nabla_x f &= z \quad (t,x) \in [0,1] \times \Omega, \\ f(0,\cdot) &= T, \end{aligned}$$

evaluated at $t = 1$.

Specification of regularizers

- Typically, we choose $\mathcal{E}_1 = \|\cdot\|^2_{L^2(\Omega)}$.
- $\mathcal{E}_2$ should be a convex, lower semi-continuous regularizer such that there exists $C > 0$ with $\|v\|_V^2 \leq C\mathcal{E}_2(v)$ for all $v \in V$ (coercivity).

Common choices for $\mathcal{E}_2$ are:

- $\mathcal{E}_2(v) = \|v\|_V^2$ with a RKHS (Reproducing Kernel Hilbert space) V
- $\mathcal{E}_2(v) = \int_\Omega L[v, v] \ + \ \gamma|D^3 v|^2 \, dx$, with $\gamma > 0$ and

$$L[v, v] := \underbrace{\operatorname{tr}\left(\varepsilon(v)^2\right)}_{\text{length change}} + \underbrace{\operatorname{tr}\left(\varepsilon(v)\right)^2}_{\text{volume change}}, \quad \varepsilon(v) := \frac{1}{2}\left(\nabla v + \nabla v^T\right)$$

  - L models the behaviour of a Newtonian fluid
  - Smoothness is ensured with the second term

Alternative models

- $z = 0 \rightarrow$ flow of diffeomorphisms setting
  - not suitable for T, R with different mass
  - not suitable for defining a nonlinear structure on $L^2(\Omega)$
- Hard constraint $S(v, z) = R$
  - more common for metamorphosis than for flow of diffeomorphisms
- Different constraint

$$
\begin{aligned}
&\frac{\partial f}{\partial t} + \operatorname{div}_x(vf) = z \quad (t, x) \in [0, 1] \times \Omega, \\
&f(0, \cdot) = T
\end{aligned}
$$

Mass preservation if $z = 0$!

Remark: Relation to Optimal Transport

$z = 0$ & hard constraint & different regularizer:

Benamou-Brenier formulation of OT

$$\min_{f,v} \int_0^1 \int_\Omega f|v|^2 \,\mathrm{d}x\,\mathrm{d}t$$

$$\text{subject to} \quad \frac{\partial f}{\partial t} + \operatorname{div}_x(vf) = 0, \quad f(0,\cdot) = T, \quad f(1,\cdot) = R$$

- Convex problem via substitution $m = vf$
- Soft constraint if the images have different intensity

Euler/Lagrange viewpoint I

Euler formulation

$$\begin{aligned} &\frac{\partial f}{\partial t} + v\nabla_x f = z \quad (t,x) \in [0,1] \times \Omega, \\ &f(0,\cdot) = T, \end{aligned}$$

Lagrange formulation (Characteristic system)

$$\begin{aligned} &\frac{\partial \varphi}{\partial t}(t,x) = v(t,\varphi(t,x)) \quad (t,x) \in [0,1] \times \Omega, \\ &\varphi(0,\cdot) = \mathrm{Id}, \\ &I(t,x) = T(x) + \int_0^t z(s,\varphi(s,x))\,\mathrm{d}s \quad (t,x) \in [0,1] \times \Omega. \end{aligned}$$

Euler/Lagrange viewpoint II

- Relation via $f(t,\varphi(t,x)) = I(t,x)$.
  $\rightarrow$ regular image paths according to definition by Trouvé & Younes.
- **Lagrange to Euler**: Assuming that everything is **smooth**, we obtain

$$
\begin{aligned}
z(t,\varphi(t,x)) &= \frac{\mathrm{d}I(t,x))}{\mathrm{d}t} = \frac{\mathrm{d}f(t,\varphi(t,x))}{\mathrm{d}t}\\
&= \frac{\partial f(t,\varphi(t,x))}{\partial t} + v(t,x)\nabla_x f(t,\varphi(t,x)).
\end{aligned}
$$

- The same holds true in the setting of regular paths (weak solutions!).
- The mathematical analysis is simpler in the Lagrange setting.

Existence of solutions for flow equation

Theorem (Trouvé)

For $v \in \mathcal{V}$ there exists a global flow $\varphi_v \in C^0([0,1], C^1(\overline{\Omega}, \mathbb{R}^n))$ which solves

$$\frac{\partial \varphi_v}{\partial t}(t,x) = v(t, \varphi_v(t,x)) \quad (t,x) \in [0,1] \times \Omega,$$
$$\varphi_v(0,\cdot) = Id.$$

In particular, $\varphi_v(t,\cdot)$ is a homeomorphism for all $t \in [0,1]$. Further, if

$$v_k \rightharpoonup v^* \quad \text{in } L^2((0,1), V),$$

then

$$\varphi_{v_k} \to \varphi_{v^*} \quad \text{in } C^0([0,1] \times \overline{\Omega}).$$

Existence of minimizers

Existence of minimizers depends on the choice of regularizers.

Theorem (Trouvé & Younes)

If $\mathcal{E}_1$ and $\mathcal{E}_2$ are convex, lower semi-continuous and coercive, then there exists a minimizer of (1).

The proof applies standard arguments and weak continuity of the control-to-state operator $S(v, z)$.

- Similar arguments can be applied for the alternative models.

Riemannian structure on space of images

Metamorphosis is used to equip $L^2(\Omega)$ with a new nonlinear structure:

- For $(I, z, v) \in (L^2(\Omega))^2 \times V$ we define curves $\gamma\colon [-1, 1] \to L^2(\Omega)$ with

$$\gamma(t) = I(\mathrm{Id} - tv) + tz.$$

- Multiple v, z with same derivative $\to$ $T_I L^2(\Omega) := V \times L^2(\Omega)/N_I$, where

$$N_I := \{V \times L^2(\Omega) : v\nabla_x I = z\}.$$

- For $\dot{I} := \dot{\gamma}(0) = \overline{(v, z)} \in T_I L^2(\Omega)$, the Riemannian metric is given by

$$g_I\big(\overline{(v, z)}, \overline{(v, z)}\big) = \min_{(\tilde{v},\tilde{z})\in(v,z)+N_I} \lambda\mathcal{E}_1(\tilde{z}) + \mathcal{E}_2(\tilde{v}).$$

- Associated path energy for a regular curve $I\colon [0, 1] \to L^2(\Omega)$:

$$E(I) = \int_0^1 g_I(\dot{I}, \dot{I})\,\mathrm{d}t = \int_0^1 \min_{(v,z):\dot{I}+v\nabla_x I=z} \lambda\mathcal{E}_1(z) + \mathcal{E}_2(v)\,\mathrm{d}t$$

Numerical approaches for metamorphosis

- Shooting methods (Richardson & Younes 2016)
- Gradient descent (or Newton's method) for reduced functional, in case of LDDMM see e.g. (Mang & Ruthotto 2017)
  - Used for implementation in (Lang, N., Öktem & Schönlieb 2018) and could be also extended to the metamorphosis framework.
- Variational time discretization (Berkels, Effland & Rumpf 2015)
  - Presented now!

Remarks on numerical solution of metamorphosis

- The problem is computationally challenging and hence efficient schemes are necessary.
- Many formulations can be solved in parallel on GPU.
- Special care is necessary to avoid numerical diffusion.
- Eulerian schemes usually require small step sizes (CFL condition!).
- Recent approaches try to incorporate machine learning for better performance.
- A very general question: Discretize vs optimize first?

Contents

Time continuous energy

Recall: Continuous path model

$$\mathcal{J}(I) = \min_{v,z} \int_0^1 \int_\Omega L[v,v] + \gamma |D^m v|^2 + \frac{1}{\delta} z^2 \,\mathrm{d}x\, \mathrm{d}t$$

$$\text{subject to} \quad \dot{I} + v \nabla_x I = z$$

We want to discretize the functional in time:

- Discrete geodesic calculus (Rumpf & Wirth 2013)
  $\rightarrow$ Time discrete geodesic path model (Berkels, Effland & Rumpf 2015)

Discretizing the energy in time

Time discrete path energy

$$\mathbf{J}_K(\mathbf{I}) := \sum_{k=1}^{K} \min_{\varphi_k \in \mathcal{A}} \int_\Omega W(D\varphi_k) + \gamma |D^m \varphi_k|^2 + \frac{1}{\delta} \left(I_{k-1} \circ \varphi_k^{-1} - I_k \right)^2 \mathrm{d}x$$

Here, we have a discrete image sequence $\mathbf{I} := (I_0, \ldots, I_K)$ and

- $W\colon \mathbb{R}^{n,n} \to \mathbb{R}_+$ lower semi-continuous and $W(A) = +\infty$ if $\det A \leq 0$, e.g. the linearized elastic potential from before,
- $\mathcal{A} := \{\varphi \in (H^m(\Omega))^n : \det(D\varphi) > 0$ a.e. in $\Omega,\ \varphi(x) = x$ on $\partial\Omega\}$.

Visualization of discrete paths

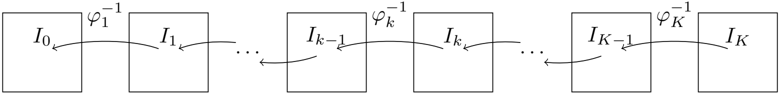

- The discrete path is a sequence of images $\mathbf{I} = (I_0, \dots, I_K)$.
- Consecutive images are related to each other via the deformations $\boldsymbol{\varphi} \coloneqq (\varphi_1, \dots, \varphi_K)$.
- Small differences between deformed and actual images are possible, modeling the source term z.
- Berkels, Effland & Rumpf (2015) have shown **existence** of time discrete geodesics and **consistency** (is explained later) of the model.
- **This model is suitable for a generalization to manifold-valued images (our work).**

Contents

Examples of manifold-valued images I

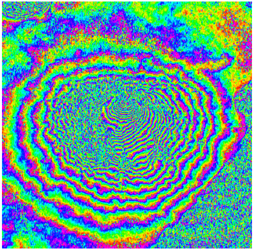

InSAR: $\mathbb{S}^1$

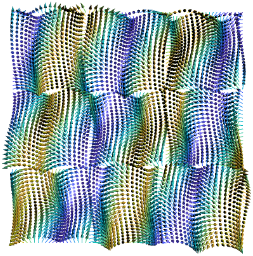

Art: $\mathbb{S}^2$

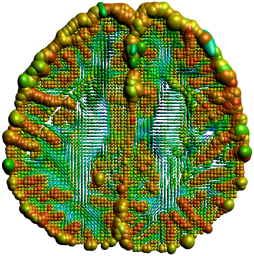

DT-MRI: SPD(3)

Image credits: Vesuvius: Rocca, Prati,Guarnierri 1997, Camino project
http://cmic.cs.ucl.ac.uk/camino

Examples of manifold-valued images II

- $\mathbb{S}^1$: phase space, InSAR (Interferometric synthetic aperture radar imaging) for volcano, HSV image space
- $\mathbb{S}^2$: directional data, chromaticity-brightness image space
- SPD(n): DT-MRI, covariance matrix information
- $\mathrm{SO}(3)$, $\mathrm{SE}(3)$: tracking, motion analysis, EBSD data (Electron Backscattered Diffraction)

More details can be found in Bergmann et al., SIAM News, 2017.

Contents

Hadamard spaces I

Definition

Hadamard space is complete geodesic metric space $(\mathcal{H}, d)$ with

$$d(x, y) \leq \|\bar{x} - \bar{y}\|$$

for comparison triangles $\Delta p, q, r$ and $\Delta \bar{p}, \bar{q}, \bar{r}$.

Comparison triangle:

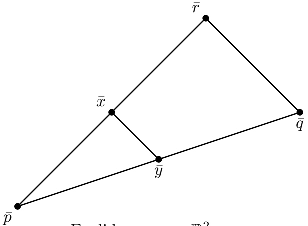

Euclidean space $\mathbb{R}^2$

$\bar{x} = \bar{p} + s(\bar{r} - \bar{p}),\ \bar{y} = \bar{p} + s(\bar{q} - \bar{p})$

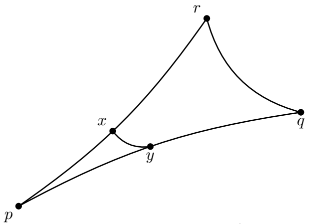

Hadamard manifold

$x = \gamma_{p,r}(s),\ y = \gamma_{p,q}(s)$

Hadamard spaces II

Examples:

- Hilbert spaces, BHV tree spaces (Billera, Holmes, Vogtmann)
- simply connected, complete, finite dimensional Riemannian manifolds of non-positive sectional curvature such as **hyperbolic spaces** or **SPD matrices** with affine invariant metric

Important:

- Hadamard spaces do **not** necessarily have a linear structure.
- Equivalents for concepts like convexity and weak convergence exist.

Good overview in the book by Bačák (2014).

Images as elements in nonlinear Lesbegue spaces I

Definition (Measurable functions)

$I : \Omega \to \mathcal{H}$ is (Lebesgue) measurable if $\{\omega \in \Omega : I(\omega) \in B\}$ is a (Lebesgue) measurable set for all $B \in \mathcal{B}$ (Borel σ-algebra on $\mathcal{H}$).

Definition ($L^p(\Omega, \mathcal{H})$ spaces)

Define $L^p(\Omega, \mathcal{H})$ as equivalence classes of measurable functions fulfilling

$$\mathrm{d}_p(I(\omega), a) < \infty \quad \text{for all } a \in \mathcal{H},$$

where

$$\mathrm{d}_p(I_1(\omega), I_2(\omega)) := \begin{cases} \left(\int_\Omega d^p(I_1(\omega), I_2(\omega)) \,\mathrm{d}\omega \right)^{\frac{1}{p}} & p \in [1, \infty), \\ \operatorname{esssup}_{\omega \in \Omega} d(I_1(\omega), I_2(\omega)) & p = \infty. \end{cases}$$

Images as elements in nonlinear Lesbegue spaces II

Hadamard manifold-valued images are interpreted as elements of $L^2(\Omega, \mathcal{H})$:

- The space $L^p(\Omega, \mathcal{H})$, $p \in [1, \infty]$, is in general not linear!
- $L^p(\Omega, \mathcal{H})$, $p \in [1, \infty]$, is a complete metric space and if $p = 2$ it is also a Hadamard space.
- $C(\Omega, \mathcal{H})$, i.e. the space of continuous maps from Ω to $\mathcal{H}$, is dense in $L^p(\Omega, \mathcal{H})$ if $\mathcal{H}$ is locally compact (N., Persch, Steidl 2018).
- $L^2(\Omega, \mathcal{H})$ is well suited for optimization due to the Hadamard space structure.

Contents

Time discrete model for Hadamard manifolds

Recall: Time discrete energy for $\mathbf{I} \in L^2(\Omega)^{K+1}$

$$\mathbf{J}_K(\mathbf{I}) := \sum_{k=1}^{K} \min_{\varphi_k \in \mathcal{A}} \int_\Omega W(D\varphi_k) + \gamma |D^m \varphi_k|^2 + \frac{1}{\delta} \left(I_{k-1} \circ \varphi_k^{-1} - I_k \right)^2 \, \mathrm{d}x$$

How does this generalize to manifold-valued images?

Time discrete energy for $L^2(\Omega, \mathcal{H})^{K+1}$

$$\mathbf{J}_K(\mathbf{I}) := \sum_{k=1}^{K} \min_{\varphi_k \in \mathcal{A}} \int_\Omega W(D\varphi_k) + \gamma |D^m \varphi_k|^2 + \frac{1}{\delta} d(I_{k-1} \circ \varphi_k^{-1}, I_k)^2 \, \mathrm{d}x$$

Existence of discrete optimal paths

Time discrete "geodesics"

Curves minimizing the energy $\mathbf{J}_K$ with fixed initial and end image:

$$\mathbf{I}_K := \operatorname{argmin}_{\mathbf{I}\in L^2(\Omega,\mathcal{H})^{K+1}} \mathbf{J}_K(\mathbf{I})$$
$$\text{subject to} \quad I_0 = T,\ I_K = R.$$

Theorem (Existence of minimizers; N., Persch, Steidl 2018)

Let $T, R \in L^2(\Omega,\mathcal{H})$ and $K \geq 2$. Then, there exists a time discrete geodesic $\hat{\boldsymbol{I}} \in L^2(\Omega,\mathcal{H})^{K+1}$ with corresponding optimal deformations $\boldsymbol{\varphi_K} \in \mathcal{A}^K$.

Proof Steps

1. For fixed $\boldsymbol{I} \in \left(L^2(\Omega,\mathcal{H})\right)^{K-1}$ the problem **decouples** into K registration problems:

$$\mathcal{R}(\varphi_k; I_{k-1}, I_k) := \int_\Omega W(D\varphi_k(x)) + \gamma|D^m\varphi_k(x)|^2 \,\mathrm{d}x + \mathrm{d}_2^2(I_{k-1}\circ\varphi_k^{-1}, I_k).$$

2. For fixed $\boldsymbol{\varphi} \in \mathcal{A}^K$ the problem **reduces**:

$$\mathbf{J}_{\boldsymbol{\varphi}}(\boldsymbol{I}) := \sum_{k=1}^{K} \mathrm{d}_2^2(I_{k-1}\circ\varphi_k^{-1}, I_k) \quad \text{subject to} \quad I_0 = T,\ I_K = R.$$

   $\rightarrow$ unique solution is given by interpolation on geodesics

3. Combine both steps to show the existence of a minimizer for the whole functional.

References for first part: Modersitzki 2004, 2009

Consistency: From discrete to continuous paths I

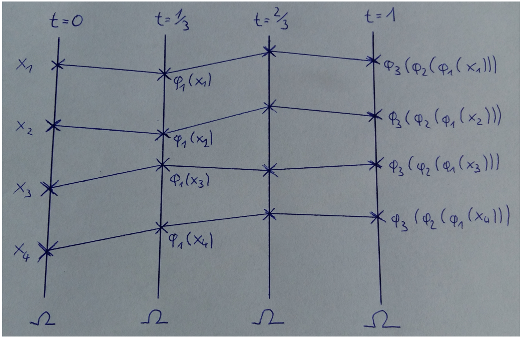

- Linear interpolation & sequence $\varphi_K \in \mathcal{A}^K$:
  $\rightarrow$ velocity field $v_K \in L^2((0,1), V)$
  $\rightarrow$ piecewise linear discrete trajectories

Consistency: From discrete to continuous paths II

- Geodesic interpolation & discrete trajectories & sequence of images $\mathbf{I}_K \in L^2(\Omega)^{K+1}$:
  $\to$ Extension to $I_K \in L^2((0,1), L^2(\Omega))$
- Distance $d(\mathbf{I}_{K,k-1}(x), \mathbf{I}_{K,k} \circ \varphi_{K,k}(x))$ & discrete trajectories:
  $\to$ "source" term $z_K \in L^2((0,1), L^2(\Omega))$
- Characteristic system is somehow unhandy (explained later) and needs to be changed!
- All tools for consistency are now defined.

Characteristic system

Recall: Characteristic system (Euclidean)

$$\frac{\partial \varphi}{\partial t}(t,x) = v(t,\varphi(t,x)) \quad (t,x) \in [0,1] \times \Omega,$$
$$\varphi(0,\cdot) = \mathrm{Id},$$
$$I(t,x) = T(x) + \int_0^t z(s,\varphi(s,x))\,\mathrm{d}t \quad (t,x) \in [0,1] \times \Omega.$$

Generalization to manifolds is not straight forward!

Modified characteristic system

Modified characteristic system

$$\frac{\partial \varphi}{\partial t}(t,x) = v(t,\varphi(t,x)) \quad (t,x) \in [0,1] \times \Omega,$$
$$\varphi(0,\cdot) = \mathrm{Id},$$
$$d\big(I(t,\varphi(t,\cdot)), I(s,\varphi(s,\cdot))\big) \le \int_t^s z(r,\varphi(r,\cdot))\,\mathrm{d}r \quad \text{for all } t < s \in [0,1].$$

- "Equivalent" to the previous formulation in the Euclidean setting.
- The "source" term is still in $L^2(\Omega)$!
- No tangent spaces involved in the last equation.
- Continuous paths (I_K, v_K, z_K) are a solution of the modified characteristic system.

Time continuous energy for manifold-valued image paths

Energy functional

$$\mathcal{J}(I) := \min_{(v,z)\in\mathcal{C}(I)} \int_0^1 \int_\Omega L[v,v] + \gamma |D^m v|^2 + \frac{1}{\delta} z^2 \,\mathrm{d}x\,\mathrm{d}t,$$

with

$$\mathcal{C}(I) := \{(v,z) \in \mathcal{V} \times \mathcal{Z} \colon (v,z) \text{ is a solution of characterstic system}\}.$$

- The constraint $C(I)$ is weakly closed.
- Standard arguments imply the existence of optimal (v,z).

Consistency with time discrete metamorphosis model

Theorem (Consistency; Effland, N., & Rumpf 2019)

Let $T, R \in L^2(\Omega)$ and let W additionally satisfy a consistency condition. For every $K \in \mathbb{N}$ let $\mathbf{I}_K \in L^2(\Omega)^{K+1}$ be a time discrete geodesic.
Then, a subsequence of $(I_K)_{k\in\mathbb{N}}$ converges weakly in $L^2((0,1) \times \Omega, \mathcal{H})$ to a minimizer I of the continuous path energy $\mathcal{J}$ subject to $I(0,\cdot) = T$ and $I(1,\cdot) = R$ as $K \to \infty$, and the associated sequence of discrete energies converges to the continuous path energy.

In particular, this implies that geodesic paths for the time continuous model exist!

Contents

Implementation Details I

- Alternating minimization over I, φ. Registration problems are solved with Quasi-Newton method.
- All involved interpolations are for manifold data: Karcher means, parallel transport ...
  $\rightarrow$ **MVIRT Toolbox** by Bergmann & Persch (MATLAB & Julia)
- Spatial discretization: Finite differences on staggered grid

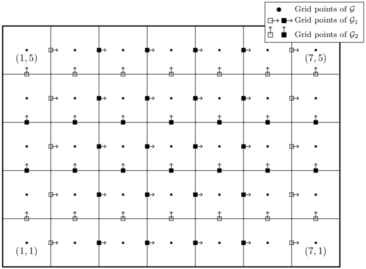

Implementation Details II

- Problem is non-convex $\rightarrow$ multiscale technique:

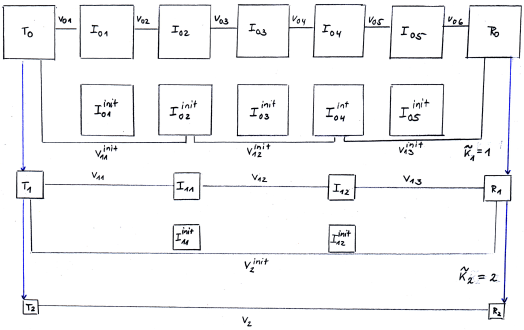

Morphing path for artificial SPD(2) images

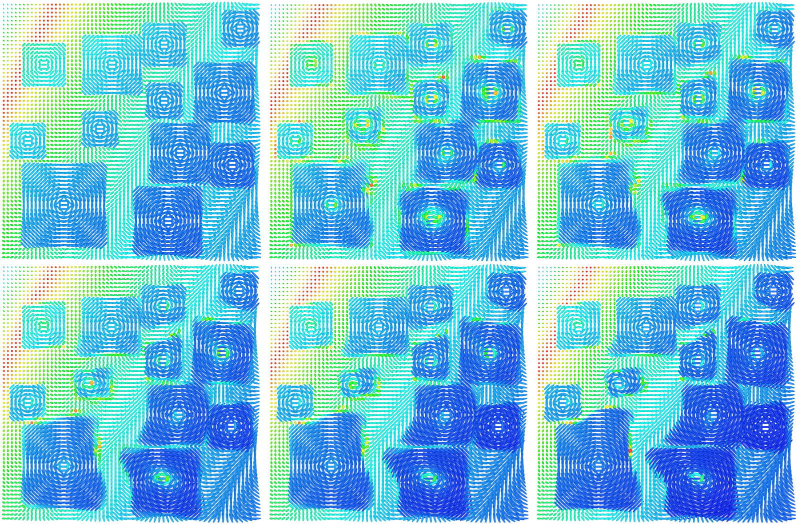

Morphing path between a part of the Camino dataset

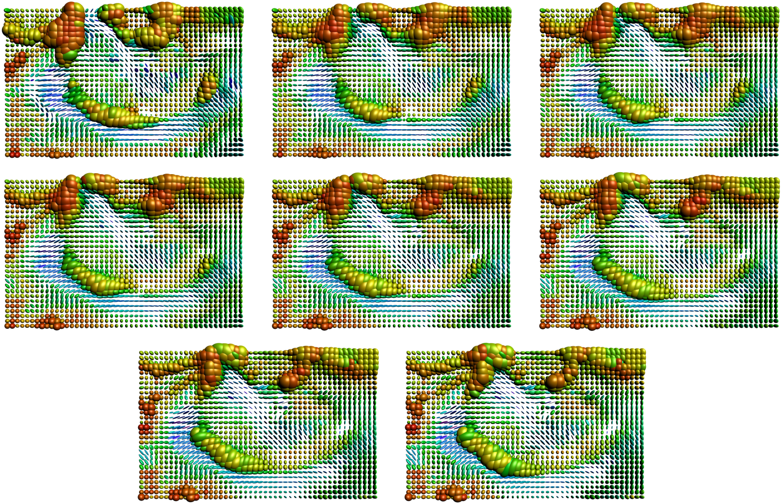

http://cmic.cs.ucl.ac.uk/camino

Morphing paths in different color spaces I

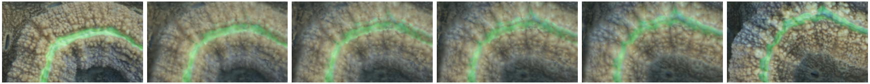

RGB color model with $\mathbb{R}^3$

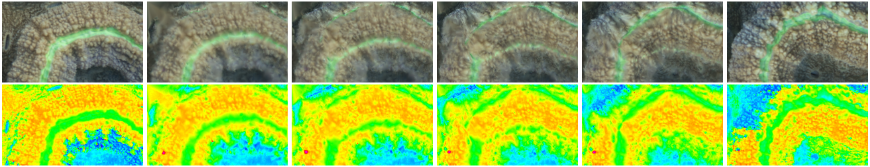

Hue-Saturation-Value color model with $\mathbb{S}^1$ and $\mathbb{R}^2$

Morphing paths in different color spaces II

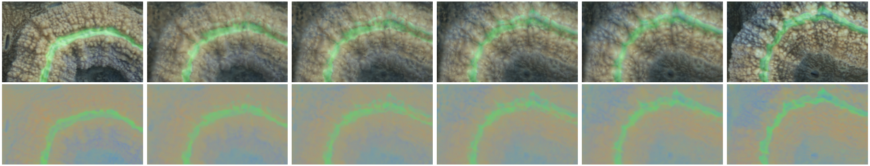

Cromaticity-Brightness color model with $\mathbb{S}^2$ and $\mathbb{R}^1$

Contents

Introduction

Back to gray-valued images!


Given template

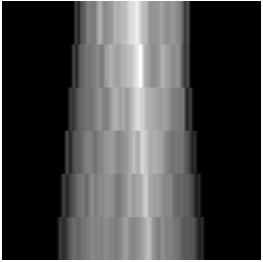
Given sinogram

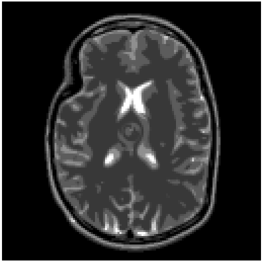
Unknown target

Only very few angles available!

$\rightarrow$ How can we use the given information for reconstruction?

Framework

- $K\colon L^2(\Omega) \to Y$ is some (not necessarily linear) observation operator and Y is the observation space, e.g. the Radon transform.
- $g \in Y$ is the known observation, e.g. the sinogram.
- Unknown target data $f \in L^2(\Omega)$, related to g via

  $$K(f) = g + n^\delta,$$

  where n^δ denotes unknown noise.
- Some prior *template* information $f_0 \in L^2(\Omega)$ about the target data f.
- The problem is usually severely ill-posed, especially for sparse data.

Reconstruction model I

Reconstruction functional

Let $\lambda > 0$ and $\mathcal{E}\colon L^2(\Omega) \to \mathbb{R}$ be some regularizer. Our proposed reconstruction model reads as

$$\min_{v \in \mathcal{V}} \int_0^1 \lambda \mathcal{E}(v(t,\cdot))\,\mathrm{d}t + D(K(S(v)), g).$$

Here, $S\colon \mathcal{V} \to L^2(\Omega)$ denotes the solution at $t = 1$ of either

$$\begin{aligned} \frac{\partial f}{\partial t} + v \nabla_x f &= 0 \quad (t,x) \in [0,1] \times \Omega,\\ f(0,\cdot) &= f_0, \end{aligned}$$

or

$$\begin{aligned} \frac{\partial f}{\partial t} + \operatorname{div}_x(vf) &= 0 \quad (t,x) \in [0,1] \times \Omega,\\ f(0,\cdot) &= f_0. \end{aligned}$$

Reconstruction model II

- Model with $D = \ell^2$ proposed by Chen & Öktem (2018).
- No source term z, since it creates reconstruction artifacts.
- **New:** $D =$ "Normalized cross-correlation"
  $\rightarrow$ enables method to deal with intensity differences
- **New:** We choose $\mathcal{E}$ as a Sobolev type regularizer $\mathcal{E}$, e.g.

$$\mathcal{E}(v) := \frac{1}{2} \int_\Omega \|\Delta v\|^2 \, \mathrm{d}x.$$

- Our implementation builds on LagLDDMM (Mang & Ruthotto, 2017) and the FAIR toolbox, hence **very flexible!**
- Efficient implementation with minimal **numerical diffusion** is very important in the reconstruction setting.

FAIR is described in the corresponding book (Modersitzki, 2009).

Normalized cross-correlation (NCC)

Definition (Variant of NCC)

For some Hilbert space Y and $\mathbf{f},\mathbf{g} \in Y$, the normalized cross-correlation $D_{\mathrm{NCC}}\colon Y \setminus \{0\} \times Y \setminus \{0\} \to [0,1]$ is defined as

$$D_{\mathrm{NCC}}(\mathbf{f},\mathbf{g}) = 1 - \frac{\langle \mathbf{f},\mathbf{g}\rangle^2}{\|\mathbf{f}\|_Y^2 \|\mathbf{g}\|_Y^2}.$$

- D_{NCC} is continuous in each argument
- D_{NCC} is invariant to a scaling $c\mathbf{f}$ with $c \in \mathbb{R}$
- $D_{\mathrm{NCC}}(\mathbf{f},\mathbf{g}) = 0$ only implies $\mathbf{f} = c\mathbf{g}$, with $c \in \mathbb{R} \to$ no real distance
- D_{NCC} is differentiable in the first variable with derivative

$$\frac{\partial}{\partial \mathbf{f}} D_{\mathrm{NCC}}(\mathbf{f},\mathbf{g}) = -\frac{2(\mathbf{f}^\top \mathbf{g})\mathbf{g}}{\|\mathbf{f}\|^2\|\mathbf{g}\|^2} + \frac{2(\mathbf{f}^\top \mathbf{g})^2\mathbf{f}}{\|\mathbf{f}\|^4\|\mathbf{g}\|^2}$$

Contents

Computation of control-to-state operator

- First discretize then optimize + Lagrange formulation
- Functions are discretized using finite differences.
- Off-grid values are computed with linear interpolation.
- ODE for coordinate transform φ is solved with RK4 method.
  - solver can be differentiated efficiently
  - other methods can be used if efficiently differentiable
- Differentiating ODE solver w.r.t. v is related to automatic differentiation.
- Continuity equation can be solved with a particle-in-cell method.
- Now, we differentiate the control-to-state operator S w.r.t. v for explicit Euler as ODE solver, works similar for RK4!
  $\rightarrow$ Quasi-Newton method

Derivative of S for explicit Euler as ODE solver

- I is a linear interpolator for off-grid values. We obtain

$$\frac{\partial}{\partial \mathbf{v}}\varphi(t_{k+1},\mathbf{x}_c) = \frac{\partial}{\partial \mathbf{v}}\varphi(t_k,\mathbf{x}_c) + \Delta t\,\frac{\partial}{\partial \mathbf{v}}\mathbf{I}(\mathbf{v},t_k,\varphi(t_k,\mathbf{x}_c)) + \Delta t\,\frac{\partial}{\partial \varphi}\mathbf{I}(\mathbf{v},t_k,\varphi(t_k,\mathbf{x}_c))\frac{\partial}{\partial \mathbf{v}}\varphi(t_k,\mathbf{x}_c).$$

- Let φ^{-1} denote the spatial inverse, i.e. the flow backward in time. Then, the chain rule implies

$$\frac{\partial}{\partial \mathbf{v}}\mathbf{S}(\mathbf{v}) = \nabla_x \mathbf{f}_0(\varphi^{-1}(1,\mathbf{x}_c))\frac{\partial}{\partial \mathbf{v}}\varphi^{-1}(1,\mathbf{x}_c).$$

  - $\frac{\partial}{\partial \mathbf{v}}\varphi^{-1}(1,\mathbf{x}_c)$ is computed in the Euler scheme together with $\varphi^{-1}(1,\mathbf{x}_c)$

Difference between constraints

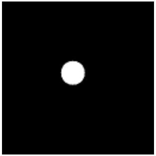

(a) Template image.

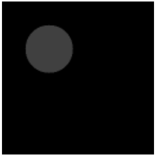

(b) Unknown image.

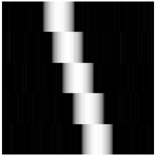

(c) Measured noisy data.

(d) Transport equation, SSIM 0.880.

(e) Continuity equation, SSIM 0.922.

Measurements are from five directions with angles equally distributed in $[0, 90]$ degrees.

Synthetic data

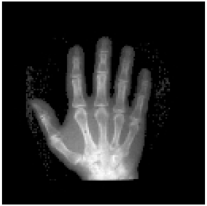

(a) Template image.

(b) Unknown image.

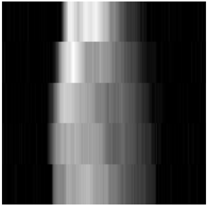

(c) Measured noisy data.

(d) Reconstruction, SSIM 0.562.

Measurements are from five directions with angles equally distributed in $[0, 75]$ degrees. Results are shown for transport equation.

Images are from FAIR toolbox.

Synthetic data

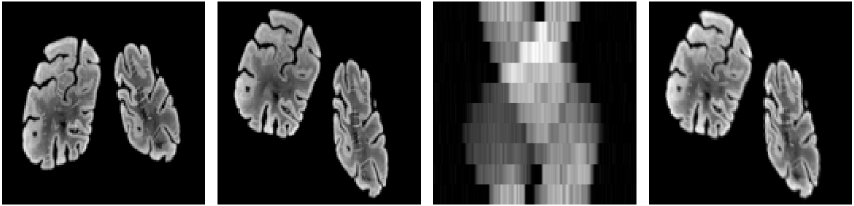

(a) Template image.

(b) Unknown image.

(c) Measured noisy data.

(d) Reconstruction, SSIM 0.913.

Measurements are from ten directions with angles equally distributed in $[0, 180]$ degrees. Results are shown for transport equation.

Images are from FAIR toolbox.

Real sinogram data from walnut

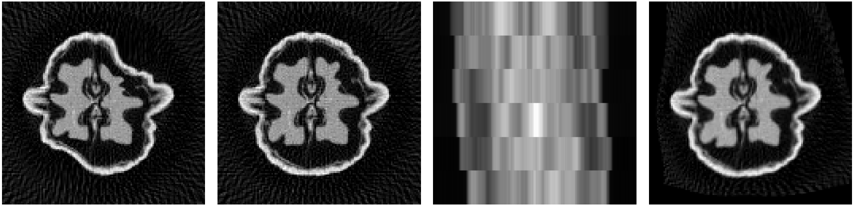

(a) Template image (synthetic).

(b) Unknown image.

(c) Measured Radon transform data.

(d) Reconstruction, SSIM 0.992.

Measurements are from six directions with angles equally distributed in $[0, 180]$ degrees. Results are shown for transport equation.

The data is taken from K. Hämäläinen et al. (2015).

Synthetic 3D data

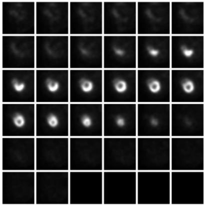

(a) Template image.

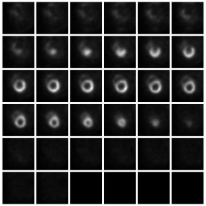

(b) Unknown image.

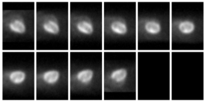

(c) Measured noisy data.

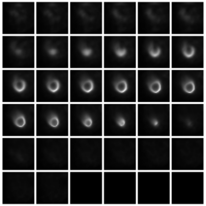

(d) Reconstruction, SSIM 0.913.

Measurements are from ten directions with angles equally distributed in $[0, 180]$ degrees. Results are shown for transport equation.

Images are from FAIR toolbox.

Conclusions

Our Contribution:

- Time discrete metamorphosis model for Hadamard manifolds
  - Generalization of Euclidean model
  - Existence of time discrete geodesics
  - Proposed time continuous model
  - Consistency of time discrete model
- Template based solution of inverse problems
  - based on LDDMM
  - D_{NCC} as data term $\to$ robustness w.r.t. different intensities
  - extension to 3D & real data

Questions?

Relevant own work

S. Neumayer, J. Persch, G. Steidl (2018)
Morphing of manifold-valued images inspired by discrete geodesics in image spaces.
SIAM J. Imaging Sci. 11(3), 1898 – 1930.

S. Neumayer, J. Persch, G. Steidl (2018)
Regularization of inverse problems via time discrete geodesics in image spaces.
ArXiv preprint #1805.06362, to appear in Inverse Problems.

L. Lang, S. Neumayer, O. Öktem, C. Schönlieb (2018)
Template-based image reconstruction from sparse tomographic data.
ArXiv preprint #1810.08596.

A. Effland, S. Neumayer, M. Rumpf (2019)
Convergence of the time discrete metamorphosis model on Hadamard manifolds.
ArXiv preprint #1902.10930.